Acyl-CoA thioesterase-2 facilitates mitochondrial fatty acid oxidation in the liver[S]

Cynthia Moffat,* Lavesh Bhatia,[1,*] Teresa Nguyen,[1,*] Peter Lynch,* Miao Wang,[†] Dongning Wang,[§] Olga R. Ilkayeva,[§] Xianlin Han,[†] Matthew D. Hirschey,[§] Steven M. Claypool, and Erin L. Seifert[2,*]**

Department of Pathology, Anatomy, and Cell Biology,* Thomas Jefferson University, Philadelphia, PA 19107; Diabetes and Obesity Research Center,[†] Sanford-Burnham Medical Research Institute, Orlando, FL 32827; Sarah W. Stedman Nutrition and Metabolism Center,[§] Duke University Medical Center, Durham, NC 27710; and Department of Physiology,** Johns Hopkins School of Medicine, Baltimore, MD 21205

Abstract Acyl-CoA thioesterase (Acot)2 localizes to the mitochondrial matrix and hydrolyses long-chain fatty acyl-CoA into free FA and CoASH. Acot2 is expressed in highly oxidative tissues and is poised to modulate mitochondrial FA oxidation (FAO), yet its biological role is unknown. Using a model of adenoviral Acot2 overexpression in mouse liver (Ad-Acot2), we show that Acot2 increases the utilization of FA substrate during the daytime in ad libitum-fed mice, but the nighttime switch to carbohydrate oxidation is similar to control mice. In further support of elevated FAO in Acot2 liver, daytime serum ketones were higher in Ad-Acot2 mice, and overnight fasting led to minimal hepatic steatosis as compared with control mice. In liver mitochondria from Ad-Acot2 mice, phosphorylating O_2 consumption was higher with lipid substrate, but not with nonlipid substrate. This increase depended on whether FA could be activated on the outer mitochondrial membrane, suggesting that the FA released by Acot2 could be effluxed from mitochondria then taken back up again for oxidation. This circuit would prevent the build-up of inhibitory long-chain fatty acyl-CoA esters. Altogether, our findings indicate that Acot2 can enhance FAO, possibly by mitigating the accumulation of FAO intermediates within the mitochondrial matrix.—Moffat, C., L. Bhatia, T. Nguyen, P. Lynch, M. Wang, D. Wang, O. R. Ilkayeva, X. Han, M. D. Hirschey, S. M. Claypool, and E. L. Seifert. **Acyl-CoA thioesterase-2 facilitates mitochondrial fatty acid oxidation in the liver. *J. Lipid Res.* 2014.** 55: **2458–2470.**

Supplementary key words β-oxidation • mitochondria • mitochondrial thioesterase • mitochondrial proton leak • cardiolipin • mouse • acyl-coenzyme A

Pathophysiological mechanisms that underlie metabolic dysfunction such as insulin resistance and nonalcoholic fatty liver disease are complex. A role for mitochondrial FA oxidation (FAO) as a driver of dysfunction has been postulated (1–3), yet the mechanistic link between cellular metabolic dysfunction and mitochondrial FAO remains poorly defined (2). Insight would be gained by a better understanding of FAO. In particular, the modulation of β-oxidation substrates and intermediates by mechanisms within the mitochondria is poorly understood, but is of interest in the context of evidence suggesting that long-chain fatty acyl-CoA esters can inhibit FAO (4–6).

Acyl-CoA thioesterases (Acots) in mitochondria, by virtue of their major substrates (long-chain fatty acyl-CoAs) and hydrolase activity which generates FA anion and free CoASH, have the potential to modulate the levels of FAO substrates and intermediates, and consequently to modulate FAO. The Acots are classified as type I or II based on catalytic domain structure, and localize to the cytosol, peroxisomes, and mitochondria. The mitochondrial Acots are Acot2 (mitochondrial matrix) (7), Acot9 (matrix) (8), Acot15/Them5 (matrix) (9), Acot11/Them1 (outside the matrix) (10), and Acot13/Them2 (outside the matrix) (11). All are type II thioesterases except for Acot2. The only matrix-localized Acot for which a functional role has been delineated is Acot15. Its germline deletion in mice

This work was supported by funds from an American Heart Association Scientist Development Grant #13SDG14380008 and Thomas Jefferson University, Department of Pathology to E.L.S.; University of Pennsylvania Mouse Phenotyping, Physiology, and Metabolism Core [National Institutes of Health (NIH) Grant P30 DK19525]; NIH Grant RO1 HL108882 to S.M.C.; NIH Grant RO1 GM105724 to X.H.; American Heart Association Grants #12SDG8840004 and #12IRG9010008 and NIH Grants RO1 AA022146 and R01AG045351 to M.D.H.

Manuscript received 7 January 2014 and in revised form 28 July 2014.

Published, JLR Papers in Press, August 11, 2014
DOI 10.1194/jlr.M046961

Abbreviations: Acot, acyl-CoA thioesterase; Ad-Acot2, model of adenoviral Acot2 overexpression in mouse liver; CL, cardiolipin; CPT, carnitine palmitoyltransferase; ECAR, extracellular acidification rate, FAO, FA oxidation; JO_2, O_2 consumption; LM, liver medium; MCoA, myristoyl-CoA; MLCL, monolysocardiolipin; NEFA, nonesterified FA; NIH, National Institutes of Health; PCarn, palmitoyl-L-carnitine; PCoA, palmitoyl-CoA; RCR, respiratory control ratio; RQ, respiratory quotient; Tg, triglyceride; Them2/5: Thioesterase superfamily member 2/5; VO_2, whole-body O_2 consumption.

[1] L. Bhatia and T. Nguyen contributed equally to this work.

[2] To whom correspondence should be addressed.
e-mail: Erin.Seifert@Jefferson.edu

[S] The online version of this article (available at http://www.jlr.org) contains supplementary data in the form of text, six figures, and one table.

lowered FAO and pyruvate oxidation and increased the level of monolysocardiolipin (MLCL) in liver mitochondria (9). MLCL is derived from the mitochondrial-specific phospholipid, cardiolipin (CL) (12). Because the major substrate for Acot15 is linoleoyl-CoA, and linoleic acid is the predominant acyl side chain in CL, it was concluded that the broad changes in mitochondrial function with Acot15 deletion reflected changes in CL metabolism (9).

Similar to Acot15, Acot2 is expressed in the liver, albeit at low levels, and is also expressed in cardiac and skeletal muscle (13–17), and is upregulated by fasting, streptozotocin-induced diabetes, and peroxisome proliferator-activated receptor agonists (13, 15–17). Its major substrates are palmitoyl-CoA (PCoA) and myristoyl-CoA (MCoA) (18), which positions Acot2 as a potential regulator of long-chain fatty acyl-CoA entry into FAO. While a role for Acot2 has been defined in steroidogenic cells (19, 20), its role in highly oxidative tissues is unknown. Here we investigated the biological role of Acot2 in nonsteroidogenic cells. To this end, we overexpressed Acot2 in the liver of mice [model of adenoviral Acot2 overexpression in mouse liver (Ad-Acot2)]. Ad-Acot2 mice had higher FA utilization during the rest phase of the day, but readily switched to carbohydrate oxidation at night. In isolated Ad-Acot2 liver mitochondria, phosphorylating O_2 consumption (JO_2) was elevated with lipid substrate, but not nonlipid substrate. While the MLCL pool was expanded in Ad-Acot2 liver mitochondria, total CL was unchanged. Overall our findings suggest that Acot2 enhances FAO. Unlike Acot15, the influence of Acot2 on mitochondrial substrate oxidation is specific to FAO and may be independent of changes in CL.

MATERIALS AND METHODS

Reagents

Unless otherwise stated, all reagents were purchased from Sigma-Aldrich.

Mice, adenoviruses, and adenoviral injection

All protocols were approved by the Thomas Jefferson University Institutional Animal Care and Use Committee. Experiments were performed on 10–13-week-old male C57BL/6J mice from our breeding colony. Mice were maintained on a 12-12 h light-dark cycle (lights on: 7:00 AM to 7:00 PM) and ad libitum fed a standard diet (LabDiet 5001, Purina). Some mice were fasted overnight (7:00 PM to 9:00 AM). Adenoviruses harboring mouse Acot2 cDNA driven by the cytomegalovirus promoter (Ad-Acot2), or the cytomegalovirus promoter only (control: Ad-Ctrl), were generated, double Cs^+ purified, and the viral titer was determined (Vector Biolabs, Philadelphia, PA). Adenoviruses (2×10^9 pfu/mouse) diluted in saline were administered via the tail vein. Mice were monitored for several hours postinjection, and did not react adversely to the injection. Mice were studied 4–7 days postinjection.

Indirect calorimetry, food intake, and spontaneous activity analysis

Whole-body JO_2 (VO_2) and CO_2 production, food intake, and locomotor activity were monitored in mice 5–6 days post adenovirus injection using the Comprehensive Lab Animal Monitoring System (Columbus Instruments, Columbus, OH). Mice were housed individually and were allowed to acclimatize to the setup prior to data collection.

Analyses of metabolites in serum, blood, and tissue

All samples were harvested at ~9:00 AM, unless otherwise stated, from fed or fasted mice. Mice were anesthetized with isofluorane, then blood was withdrawn via the inferior vena cava using a 23 gauge needle, allowed to clot at room temperature, and then centrifuged at 4,000 *g* to obtain serum. Nonesterified FAs (NEFAs) (WAKO Chemicals, Richmond, VA), triglycerides (Tgs) (Stanbio Laboratory, Boerne, TX), and β-hydroxybutyric acid (Stanbio Laboratory) were measured according to manufacturers' protocols. Hepatic Tg secretion was measured in whole blood from mice after a 5 h fast (start 10:00 AM) followed by injection of Tyloxapol (500 mg/kg) via the tail vein to inhibit Tg clearance. Blood samples were collected prior to Tyloxapol injection, and then hourly postinjection for 4 h. For Tg determination in the liver, livers (~50–100 mg each) were rapidly dissected from mice euthanized by decapitation, and then snap-frozen in liquid nitrogen until processing.

Liver mitochondria isolation

Liver mitochondria were isolated as described (21). Mice were euthanized by decapitation at ~9:00 AM. All steps were performed on ice or at 4°C. Livers were dissected, washed in liver medium (LM) [250 mM sucrose, 10 mM Tris-HCl, 0.1 mM EGTA (pH 7.4)], and then minced by razor blade. Minced tissue was suspended in LM + 0.5% defatted BSA in a Potter-Elvehjem homogenizer and processed using a motorized homogenizer (500 rpm, 12 passes). Samples were centrifuged (10 min, 600 *g*). The supernatant was centrifuged again (10 min, 600 *g*), and then for 10 min at 7,000 *g*. The pellet was resuspended in LM then washed twice. The final pellet was resuspended in a minimal volume of LM for a protein concentration of ~25 mg/ml, as determined by BCA assay (Life Technologies, Carlsbad, CA).

Isolation and culture of primary hepatocytes

Hepatocytes were isolated from mice, 7 days post adenovirus injection, by in situ retrograde perfusion of the liver and collagenase digestion. The liver was perfused [31.5 mM glucose, 100 mM NaCl, 2.5 mM KCl, 1 mM KH_2PO_4, 25 mM HEPES (pH 8.5), and 0.5 mM glutamine supplemented with an amino acid solution; at 9 ml/min, 37°C) by cannulating the inferior vena cava with outflow through the portal vein. Blood and endogenous calcium were washed out with EGTA (0.5 mM EGTA in perfusion solution). The liver was then perfused with collagenase (180 cdu/ml type I collagenase in perfusion solution). Once sufficiently digested (~10 min), the reaction was stopped by placing the liver in ice-cold buffer (perfusion solution plus 0.2% deffated BSA). Cells were gently liberated, filtered, and pelleted (40 *g*, 3 min, 4°C). Hepatocytes were seeded onto collagen-coated culture plates and cultured overnight in William's E medium plus 1 mM glutamine, 1% Penn/Strep, 25 μg/ml gentamycin, and 1 μM dexamethasone.

Bioenergetics analyses in isolated mitochondria and hepatocytes

JO_2 was measured using the Seahorse XF24 analyzer (Seahorse Bioscience, Billerica, MA). Isolated mitochondria were studied essentially according to (22). Each well of the custom microplate contained 10 ug of mitochondria suspended in mitochondrial isolation medium [70 mM sucrose, 22 mM mannitol, 10 mM KH_2PO_4, 5 mM $MgCl_2$, 2 mM HEPES, 1 mM EGTA, 0.2% defatted BSA (pH 7.4) at 37°C]. The microplate was centrifuged (2,000 *g*, 20 min, 4°C) to promote adhesion of mitochondria to

the plastic. Attachment was verified after centrifugation and again after experiments. Substrate conditions are described in the Results. Oligomycin (4 μg/ml) was used to measure leak-dependent JO_2. Hepatocytes were seeded (20,000/well) then studied within 24 h in DMEM plus 5 mM glucose. Palmitate (conjugated 3:1 with BSA) was added during the assay, followed by oligomycin (500 ng/ml), and then 1 μM antimycin to measure nonmitochondrial JO_2. The residual antimycin JO_2 was subtracted from the other rates to obtain mitochondrial JO_2. Proton-motive force was measured in mitochondria using 5 μM safranin O dye and in the presence of nigericin (0.4 μg/ml) (21).

Thioesterase activity and kinetic analysis

Samples were diluted to 20 μg/μl in mitochondrial isolation medium and subjected to five freeze-thaw cycles. Reactions were carried out in a total volume of 300 μl in reaction buffer [50 mM KCl, 10 mM HEPES (pH 7.6)] at 37°C. Samples (40 μg/well) were added to prewarmed buffer and 0.3 mM DTNB. Absorbance at 412 nm was read (every 30 s for 3 min), and then substrate was added and absorbance was measured at 412 nm (every 15 s for 5 min). Initial rates (V_0) were calculated by determining the maximal rate by iterative linear regression using at least five consecutive time points. Thioesterase activity was determined using a molecular extinction coefficient of 13,600 $M^{-1}cm^{-1}$. Enzyme kinetics was analyzed by nonlinear regression using GraphPad Prism6: values of V_0 were fitted to the Michaelis-Menten equation $V_0 = V_{max}[S]/([S] + K_m)$ where [S] is the substrate concentration, yielding the maximal velocity (V_{max}) and the Michaelis-Menten constant (K_m).

Western blotting

To prepare lysates, tissue was homogenized in RIPA buffer containing inhibitors of proteases (Roche Applied Science, Branford, CT) and phosphatases (Sigma-Aldrich), incubated on ice for 40 min, and then cleared (18,000 *g*, 15 min, 4°C). Protein concentration was determined by the BCA method. For mitochondria, an aliquot of mitochondria was placed in sample buffer immediately upon completion of the isolation procedure. Samples were loaded onto an 8 or 10% polyacrylamide gel, electrophoresed, transferred onto nitrocellulose, and blocked with Odyssey blocking buffer (LI-COR Biosciences, Lincoln, NE). All primary antibodies were diluted in TBS-T. Acot2 expression was probed using one of two different custom polyclonal antibodies (1:250 dilution, 21st Century Biochemicals or 1:2,000, a gift from Stefan Alexson, Karoliska Intitute). All other antibodies: [Abcam: carnitine palmitoyltransferase (CPT)1A 1:1,000, Complex I (39 kDa subunit) 1:1,000, Complex II (SDHA subunit) 1:10,000, Complex III (Core 1 subunit) 1:1,000, Complex IV (Cox1 subunit) 1:2,000, Complex V (α subunit) 1:1,000, prohibitin 1:1,000; Advanced Immunochemical Incorporated: GAPDH 1:12,000; BD Pharmingen: cytochrome c 1:1,000; Cell Signaling: acetylated-lysine (#9681, #9441, or #9814) 1:1,000]. Secondary antibodies (LI-COR) were diluted 1:20,000 in 5% skim milk. Protein bands were visualized using the LI-COR Odyssey3000 system.

Acyl-carnitine esters

Fed mice were euthanized by cervical dislocation at ~9:00 AM. The liver was rapidly removed and freeze-clamped within 30 s. Acyl-carnitines were measured at the Sarah W. Stedman Nutrition and Metabolism Center Mass Spectrometry Laboratory. Acyl-carnitines were analyzed by direct-injection electrospray MS/MS using a Micromass Quattro Micro LC-MS system (Waters-Micromass, Milford, MA) equipped with an autosampler (model HTS-PAL 2777; Leap Technologies, Carrboro, NC), a HPLC solvent delivery system (model 1525; Agilent Technologies, Palo Alto, CA), and a data acquisition system (MassLynx 4.0 software; Waters, Milford, MA).

Shotgun lipidomics analysis

Lipids were extracted from mitochondria by a modified Bligh and Dyer method (23). Internal standards for quantification of individual molecular species of lipid classes were added prior to extraction (23). Shotgun lipidomics analyses were performed with a QqQ mass spectrometer (TSQ Vantage; Thermo Fisher Scientific, San Jose, CA) equipped with an automated nanospray device (Triversa Nanomate; Advion Biosciences, Ithaca, NY) operated with Xcalibur software (24). Identification and quantification of lipid molecular species were performed using a multi-dimensional mass spectrometry-based shotgun lipidomics approach and automated software (25, 26).

CL and MLCL analyses by TLC

Phospholipid extraction, staining, and quantitation were performed as described (27, 28). In brief, phospholipids from 0.9 mg of mitochondria were extracted with chloroform:methanol. Chloroform-resuspended samples were loaded onto ADAMANT TLC plates (Machery-Nagel, Dueren, Germany) and resolved using chloroform:ethanol:water:triethylamine (30:35:7:35). Phospholipids were visualized with 1.3% molybdenum blue spray reagent (Sigma-Aldrich). Scanned images were analyzed using Quantity 1 software (Bio-Rad Laboratories, Hercules, CA). Phosphate concentration was determined (29).

Electron microscopy

The livers were harvested from fed and overnight fasted mice, processed for transmission electron microscopy, and analyzed morphometrically using ImageJ, and as described in (30). At least six cells were analyzed per liver. Only images containing a nucleus were analyzed. At least 150 mitochondria were analyzed per cell.

Quantitative PCR

Total RNA was extracted from liver using Trizol® (Invitrogen, Carlsbad, CA). Purified RNA was treated with RQ1 DNase (Promega, Madison, WI) at 37°C for 30 min. Total RNA concentration was measured using a Qubit® fluorometer (Invitrogen). RNA was reverse transcribed using oligo$(dT)_{20}$ primers and SuperScript III (Invitrogen). Quantitative PCR reactions for gene expression studies were performed using ITaq SYBR Green Supermix with ROX (Bio-Rad) in 20 μl reactions (20 ng cDNA/reaction). Quantitative PCR was performed using an Eppendorf Mastercycler® ep realplex. Primers were designed using Eurofins Primer Design Tool, and are described in the supplementary Methods. Custom oligos were purchased from Eurofins MGW Operon (Huntsville, AL).

Statistical analyses

Data are presented as the mean and standard error. Statistical differences were determined by unpaired *t*-test or ANOVA (followed by Tukey post hoc comparisons for $P < 0.05$ by ANOVA). $P < 0.05$ was taken as significant.

RESULTS

Model system

To determine the role of Acot2 in the liver, we overexpressed murine Acot2 via adenoviral delivery of mouse

Acot2 cDNA by tail vein injection. Western blotting analysis of liver fractions confirmed localization of the overexpressed protein to mitochondria (**Fig. 1A**). In both fed and fasted mice, we measured Acot2 protein in muscle and brain, and found no increase in Ad-Acot2 mice (not shown, see supplementary Fig. I). Fasting is known to elevate Acot2 protein in the liver, thus we compared protein levels of overexpressed Acot2 to levels from fasted mice. Fasting induced a small increase in Acot2 protein (supplementary Fig. I). Overexpressed levels were approximately three times higher than the fasted levels (supplementary Fig. I). To determine whether overexpressed Acot2 was active, we measured thioesterase activity in liver mitochondria. As expected (7), Acot2 overexpression resulted in elevated thioesterase activity when PCoA (C16:0-CoA; Fig. 1B, D), MCoA (C14:0-CoA; Fig. 1E), and to a lesser extent oleoyl-CoA (C18:1-CoA; Fig. 1C) and linoleoyl-CoA (C18:2-CoA; Fig. 1C) were used as the substrate, but not with octanoyl-CoA (C8:0-CoA; Fig. 1C). Using nonlinear regression, the K_m (at 37°C) of overexpressed Acot2 was 3.3 μM for PCoA or MCoA (Fig. 1D, E), within the range of K_m values (2.9–5.8 μM) determined for the purified rat protein (18). The K_m of thioesterase activity measured in Ad-Ctrl liver mitochondria was slightly higher (~4 μM). V_{max} was also differed between Ad-Acot2 and Ad-Ctrl mitochondria, with a lower rate in Ad-Ctrl mitochondria (Fig. 1D, E). Thioesterase activity in Ad-Ctrl liver mitochondria could derive from the activity of Acot13 [Them2, likely associated with the outer mitochondrial membrane (11)] and Acot15 [Them5, localized to the matrix (9)], however the K_m for PCoA is closer to that measured for purified Acot15 (9). Thioesterase activity in Ad-Acot2 mitochondria supplied with PCoA declined at [PCoA] > 20 μM, and thioesterase activity was only 10 ± 1.1 μmol/min/mg with 100 μM PCoA, in agreement with observations in purified rat Acot2 (18). Inhibition is unlikely to reflect PCoA micelle formation because this would not occur at 37°C for concentrations <60 μM PCoA (11). Thus the inhibition likely reflects substrate inhibition, as was proposed (18).

Studies in mice: hepatic Acot2 overexpression increases hepatic FAO

Ad libitum fed mice. To study the biological role of Acot2, Acot2 was overexpressed in ~10-week-old male C56BL/6J mice. Seven days after tail vein injection, body weight was similar in Ad-Ctrl and Ad-Acot2 mice: 26.3 ± 0.4 g (Ad-Ctrl) versus 26.2 ± 0.5 g (Ad-Acot2) on day of euthanization (n = 10/group), compared with 24.8 ± 1.1 g (Ad-Ctrl) versus 25.8 ± 0.6 g (Ad-Acot2) just prior to adenovirus injection. Adiposity was slightly lower in Ad-Acot2 mice, as determined by the weight of peri-gonadal fat pads: 0.29 ±

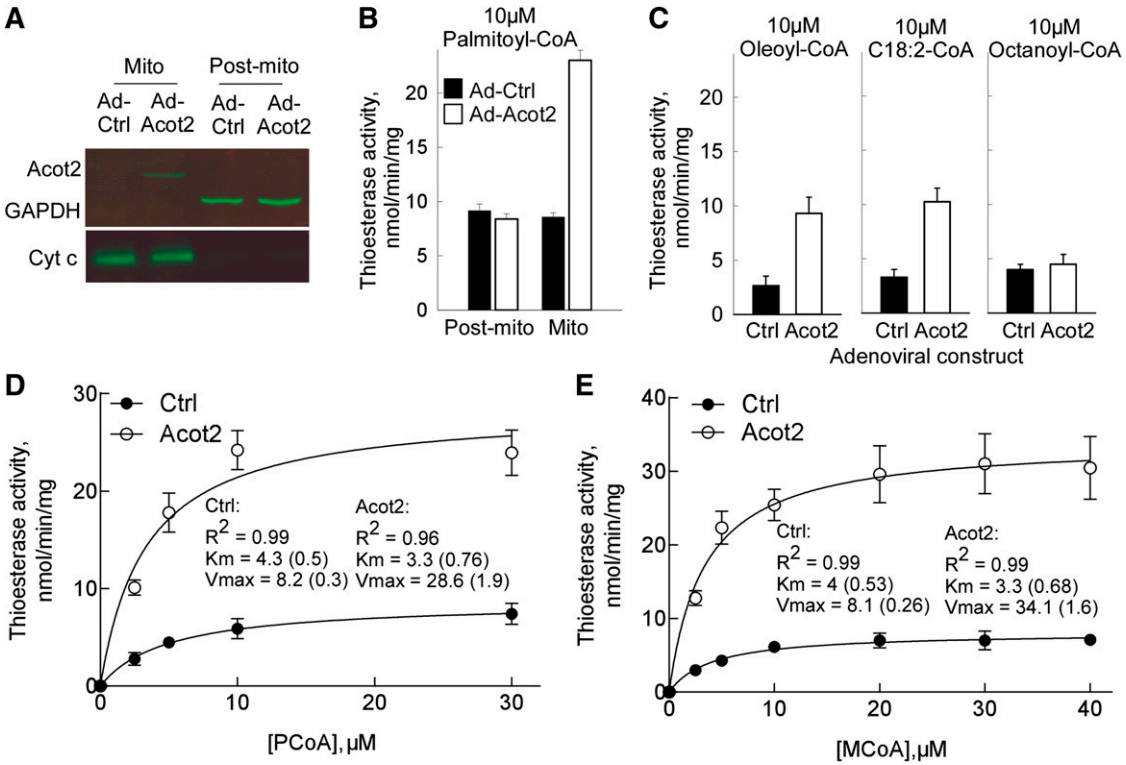

Fig. 1. Model of hepatic Acot2 overexpression. A: Western blot analysis of Acot2 protein in liver mitochondria (Mito) and in the supernatant fraction (Sup) of a mitochondrial isolation. Cytochrome c (Cyt c) was used as a marker of the Mito fraction, and GAPDH (glyceraldehyde-3-phosphate dehydrogenase) was used as a marker for the Post-mito fraction. B: Thioesterase activity (initial rates) in Mito and Post-mito fractions, in preparations from Ad-Ctrl and Ad-Acot2 liver; n = 3/group. C: Thioesterase activity (initial rates) in Mito fractions, in preparations from Ad-Ctrl and Ad-Acot2 liver; n = 3–4/group. D, E: Enzyme kinetics (initial rates) in Ad-Ctrl and Ad-Acot2 liver mitochondria, with PCoA (D) or MCoA (E). The data were fitted using nonlinear regression, from which K_m and V_{max} were calculated (values are the mean with SEM in parentheses). n = 3–4/group. B–E: Black bars (filled circles): Ad-Ctrl; open bars (open circles): Ad-Acot2; values are the mean ± SEM.

0.03 g (Ad-Ctrl) versus 0.21 ± 0.02 g (Ad-Acot2) (n = 10/group, $P = 0.001$). Both food intake and spontaneous activity were higher at night in Ad-Acot2 mice (**Fig. 2A**). VO_2 was similar between Ad-Ctrl and Ad-Acot2 mice, whether during the light or dark phases of the day (Fig. 2B). On the other hand, the respiratory quotient (RQ = CO_2 production/JO_2), which provides information on the substrate being oxidized (RQ = 0.7 for pure FAO; RQ = 1 for pure carbohydrate oxidation), was lower in Ad-Acot2 mice during the light phase of the day, and then rose to reach a level similar to that in Ad-Ctrl mice during the dark phase (Fig. 2C). The rise in RQ was not delayed in Ad-Acot2 mice. β-Hydroxybutyric acid and NEFA in serum (Fig. 2D), and Tg content in the liver (Fig. 2E) were each slightly elevated in Ad-Acot2 mice. Acyl-carnitines were also measured in whole liver from fed mice. Acetyl-carnitine and propionyl-carnitine, as well as medium- and long-chain acyl-carnitines, were higher in Ad-Acot2 liver (Fig. 2F). Finally, we noted no difference in the expression of various mitochondrial proteins, including CPT1 (which mediates the first step of long-chain fatty uptake into mitochondria), whether assayed in isolated mitochondria or liver lysates (supplementary Fig. II), or in transcript levels of the hepatic lipid synthetic enzymes (supplementary Fig. III).

Overnight-fasted mice. With overnight fasting, both Ad-Ctrl and Ad-Acot2 mice lost most of their white adipose tissue stores, and the decrease occurred with similar kinetics (**Fig. 3A**). Both groups also lost a similar amount of body mass (17.8 ± 0.8% decrease in Ad-Ctrl vs. 16.9 ± 0.8% in Ad-Acot2, n = 7/group; $P > 0.05$). As expected, upon food withdrawal at 7:00 PM, the RQ decreased rapidly toward 0.7; the extent and kinetics of the drop were similar in Ad-Ctrl and Acot2 mice (Fig. 3B). Increases in serum NEFA and in β-hydroxybutyric acid were similar between fasted Ad-Ctrl and Ad-Acot2 mice (Fig. 3C, D), whereas serum Tg was lower in Ad-Acot2 mice throughout the entire fasting period (Fig. 2E). Hepatic lipid accumulation

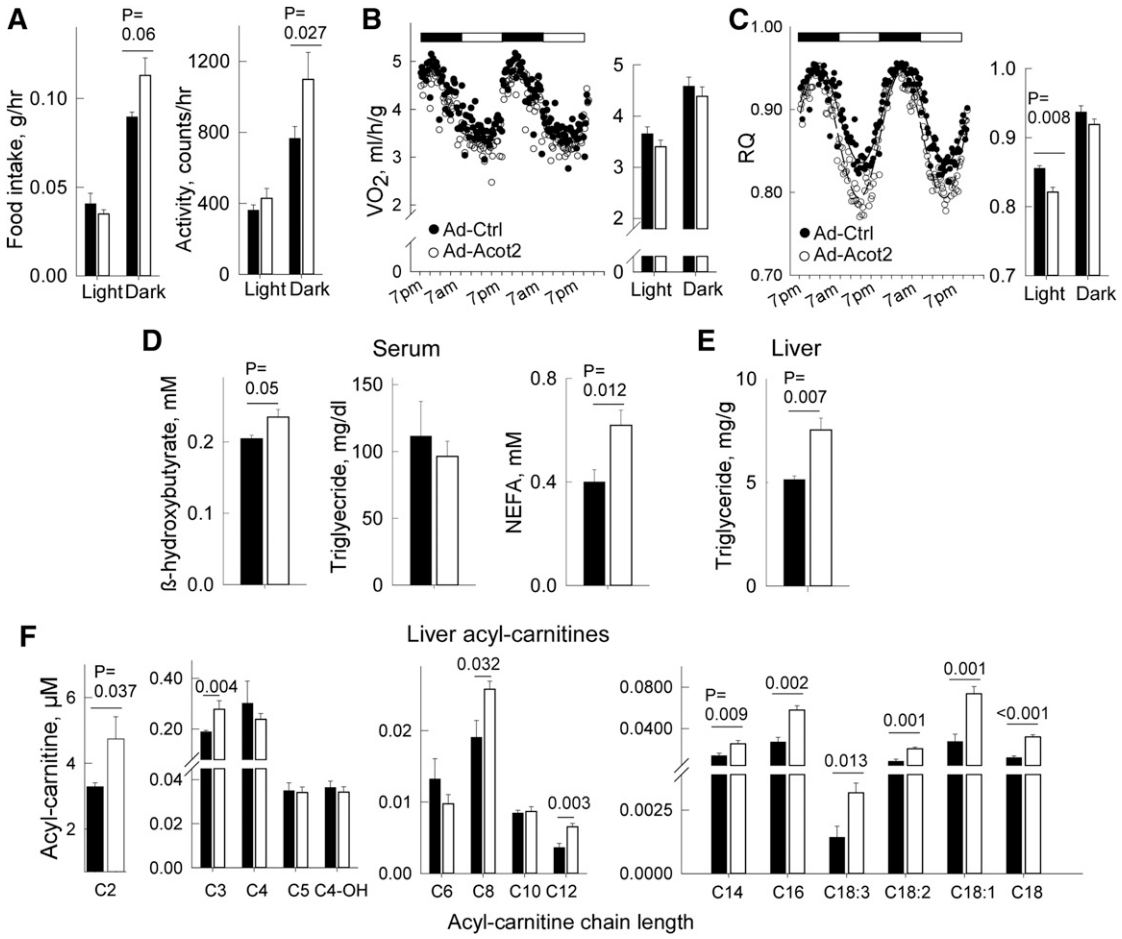

Fig. 2. Hepatic Acot2 overexpression leads to elevated FAO in vivo. CLAMS (Comprehensive Laboratory Animal Monitoring System) was used to measure food intake and spontaneous locomotor activity (A) (n = 4/group), VO_2 (B), and RQ (CO_2 production/VO_2) (C) in fed Ad-Ctrl and Ad-Acot2 mice; n = 11/group; Light and Dark refer to period of the day when lights are on (7:00 AM-7:00 PM) or off. Black and white bars above plots in (B) and (C) reflect the light and dark phases of the day. In the time series, symbols are averages/group/time point. D: Serum analysis in ad libitum-fed mice of β-hydroxybutyric acid (fed mice, n = 6/group; fasted mice, n = 8/group), NEFA (fed mice, n = 9/group; fasted mice, n = 8/group), Tg (all groups: n = 6). E: Liver Tg in ad libitum-fed fasted mice, measured biochemically (bar chart, n = 4/group) F: Acetyl-carnitine and acyl-carnitines measured in the liver from ad libitum-fed mice (n = 4/group). A–F: Bar chart: mean + SEM; black symbols/bars: Ad-Ctrl, open symbols/bars: Ad-Acot2; *P* values from unpaired *t*-test.

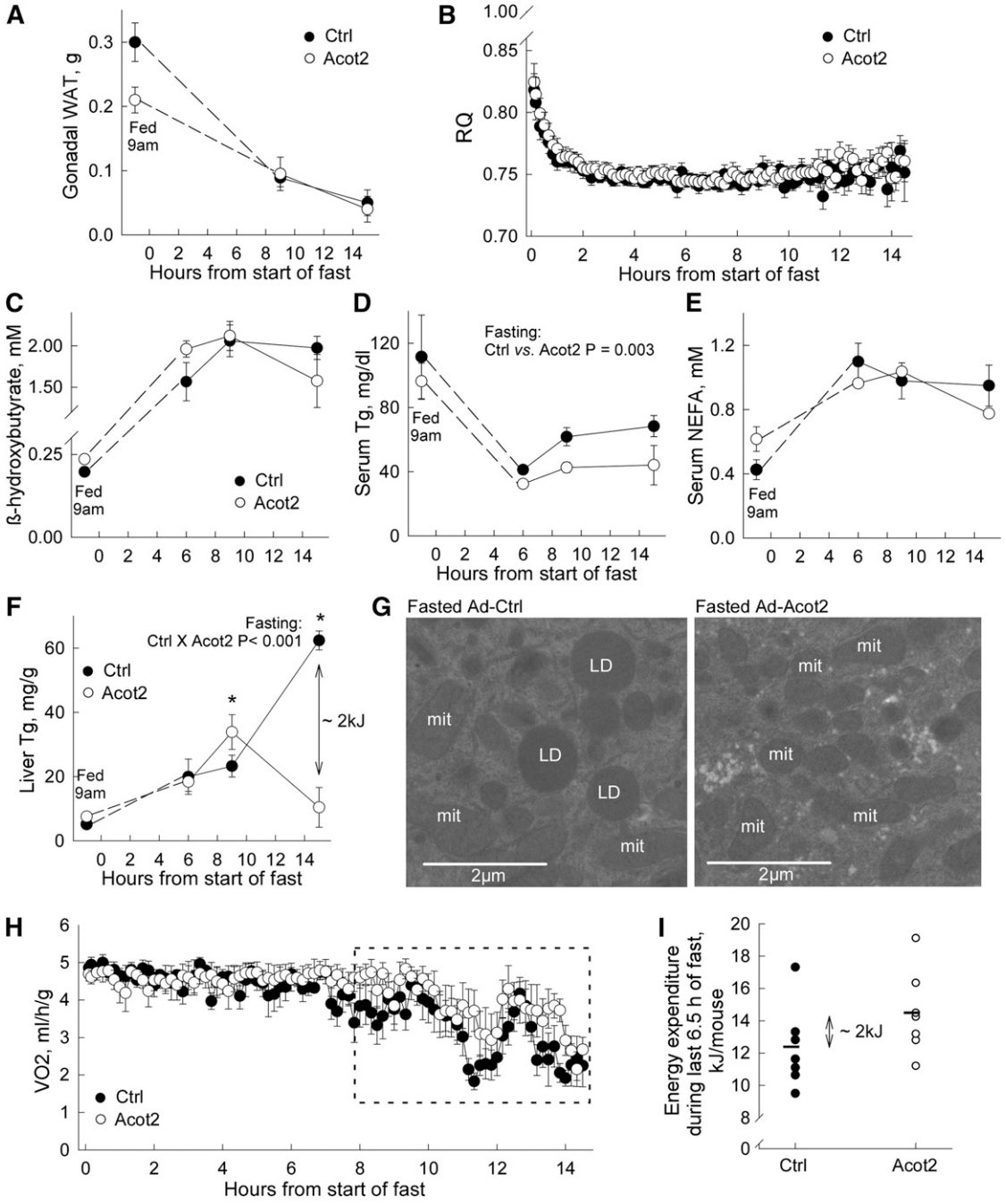

Fig. 3. Fasting depletes hepatic Tgs in Ad-Acot2 mice. A: Gonadal white adipose tissue (WAT) measured in ad libitum-fed mice (fed 9:00 AM) and in mice fasted for 9 or 15 h. B: RQ during fasting (n = 7 mice/group). C–E: Serum β-hydroxybutyric acid, Tg, and NEFA, respectively, fasted for different durations (n = 4–6/group). F: Liver Tg in fasted mice (n = 4–6/group). After 15 h of fasting, the approximate difference in the energy content of liver Tg was 2 kJ. See text for further explanation. G: Electron micrographs of the liver from fasted mice. Images are representative of those obtained for three mice/group, and were different mice from those used for biochemical analysis of liver Tg in (F). mit, mitochondria; LD: lipid droplet. H: VO_2 in fasting mice (n = 7/group). Boxed area indicates data used for analysis in (I). I: Energy expenditure per mouse was calculated by measuring VO_2 per mouse for the last 6.5 h of the fast by digitizing the entire area using identically scaled graphs for each mouse. Each circle is from an individual mouse. Bars are the average value for the group. The approximate average difference was 2 kJ. In all panels, fasting was started at 7:00 PM. In all panels except (G) and (I), values are the mean and error bars are the SEM. $*P < 0.05$, Tukey post hoc test (ANOVA showed significant genotype × time interaction).

(Fig. 3F) was similar between Ad-Ctrl and Ad-Acot2 mice during the first 6 h of the fast, then was slightly higher in Ad-Acot2 liver after 9 h of fasting. However, by the 15 h time point, liver Tg was greatly elevated in Ad-Ctrl liver but had decreased to near fed levels in Ad-Acot2 liver. The biochemical determinations of liver Tg at the 15 h time point were corroborated by electron micrographs showing abundant lipid droplets in fasted Ad-Ctrl mice, whereas lipid droplets were never seen on micrographs from Ad-Acot2 mice. Development of frank hepatic steatosis with

fasting has been reported in multiple strains of inbred mice, including C57BL/6J mice, with levels after an overnight fast (~15 h) similar to those that we observed in Ad-Ctrl liver (31). Enhanced Tg secretion from the liver would likely not explain the drop in liver Tg in Ad-Acot2 because hepatic Tg secretion tended to be higher in Ad-Ctrl mice (supplementary Fig. IV), which is consistent with the higher serum Tg in Ad-Ctrl mice (Fig. 3D). We sought evidence for greater lipid accumulation in Ad-Acot2 muscle, questioning whether lipid was being preferentially stored there instead of in the liver; however, Tg levels in gastrocnemius were similar to Ad-Ctrl levels throughout the fast (supplementary Fig. V). The levels of various mitochondrial proteins, including CPT1, were similar between Ad-Ctrl and Ad-Acot2, whether in liver lysates or isolated mitochondria (both from the 15 h time point) (supplementary Fig. II). Similar protein levels in liver lysates suggested that mitochondrial content was not different in Ad-Acot2 liver. This was supported by electron microscopy of liver sections (supplementary Fig. VI). Interestingly, while the general appearance of mitochondria, including the cristae, was normal in Ad-Acot2 liver (not shown), morphometric analysis revealed proportionately larger mitochondria in fed Ad-Acot2 liver, as indicated by a larger surface area with no change in aspect ratio. With fasting, Ad-Ctrl mitochondria lengthened, whereas the shape of Ad-Acot2 did not change (supplementary Fig. VI). The morphometric differences between Ad-Ctrl and Ad-Acot2 mitochondria are also consistent with elevated FAO in Ad-Acot2 mitochondria from fed mice, as discussed below.

The Acot2 reaction could increase the abundance of free FAs in the mitochondrial matrix, and free FAs can uncouple oxidative phosphorylation leading to energy expenditure in the absence of ATP production. This effect may become particularly pronounced during fasting, when lipids are the primary substrate for oxidation over a prolonged period of time. Thus, we measured VO_2 by indirect calorimetry in fasted mice. When the whole 15 h fasting period was considered, VO_2 was similar in Ad-Ctrl and Ad-Acot2 mice (Fig. 3H). On the other hand, when only the last ~6 h were analyzed, VO_2 tended to be higher in Ad-Acot2 mice. To determine whether higher VO_2 in Ad-Acot2 mice could account for the depletion of liver Tg (Fig. 3F), VO_2 was measured in each mouse for the last 6.5 h of the fast (boxed region in Fig. 3H). This was done by digitizing the entire area under the VO_2 trace for each mouse that was plotted on identically scaled graphs. Then the values were converted to energy expenditure per mouse. Energy expenditure per mouse tended to be higher in Ad-Acot2 mice ($P = 0.15$; $P < 0.05$ with removal of the highest value in Ad-Ctrl group). Interestingly, the difference in average energy expenditure between the Ad-Ctrl and Ad-Acot2 mice was ~2 kJ, which is similar to the difference in the energy content of hepatic Tg at the end of the fast (Fig. 3F; ~2 kJ/liver, noting that liver weights were similar in Ad-Ctrl and Ad-Acot2 mice and were ~1 g at the end of the fast). It should be noted that a 2 kJ difference would be expected to be detectable by indirect calorimetry.

Finally, given the possible role for Acot15 in CL remodeling (9), and knowing that CL plays an important role in mitochondrial function (32), we also determined whether changes in the content and composition of CL and the CL intermediate MLCL might explain differences in Ad-Ctrl and Ad-Acot2 liver. This seemed important to test also because, although oleoyl-CoA (18:1-CoA) and linoleoyl-CoA (18:2-CoA) are not the major substrates of Acot2, Acot2 overexpression more than doubled the mitochondrial thioesterase activity for these substrates (see Fig. 1), and linoleic acid, and to a lesser extent oleic acid, are major acyl side chains of CL. Quantification of CL and MLCL by MS of mitochondria from fasted mice revealed an expansion of the MLCL pool, due to increases in all MLCL species as evidenced by a greater abundance of all fatty acyl chains (**Fig. 4A**, supplementary Table I). In contrast, there were no robust changes in total CL, which was also observed using TLC analysis of mitochondria from fed and fasted mice (Fig. 4B; the low level of MLCL is below the detection limit of TLC). In addition, there was no difference between Ad-Ctrl and Ad-Acot2 mitochondria in the total abundance of phospholipids (Fig.4B).

Overall, these analyses suggest that the higher FA utilization during the daytime in ad libitum-fed Ad-Acot2 mice is unrelated to changes in mitochondrial content or CL metabolism. Hepatic depletion of Tg in fasted Ad-Acot2 mice may be due to increased energy expenditure, possibly caused by greater uncoupled respiration.

Flux studies in mitochondria and hepatocytes: Acot2 overexpression facilitates FAO and introduces a proton leak pathway

To gain further insight into the role of Acot2 in FAO, we turned to flux experiments in mitochondria and hepatocytes. Acot2 hydrolyzes long-chain fatty acyl-CoA into CoASH and free FA, and was hypothesized to facilitate mitochondrial β-oxidation by mitigating a CoASH limitation when mitochondrial FA load is high (33). Acot2 could also facilitate FA utilization if the released FA cycled in the inner mitochondrial membrane, providing a return path into the matrix for protons, thereby increasing uncoupled respiration [e.g., (34)]. To test these possibilities, a detailed bioenergetics analysis was performed in liver mitochondria and intact hepatocytes, which was also to determine whether Acot2 overexpression had broader effects on substrate oxidation.

Ad-Ctrl and Ad-Acot2 liver mitochondria (from fed mice) oxidizing pyruvate + malate had similar state 3 JO_2 rates and respiratory control ratios (RCRs) (**Fig. 5A**). There was also no difference between Ad-Ctrl and Ad-Acot2 mitochondria in the state 3 and state 4 rates with succinate as the substrate (not shown). Proton-motive force measured with pyruvate + malate, and in the presence of oligomycin, was similar between Ad-Ctrl and Ad-Acot2 mitochondria (Fig. 5A), as was citrate synthase activity (Fig. 5B).

Low and high concentrations of FA substrate were used to test whether Acot2 could play an important role when substrate load is high in Ad-Acot2 liver mitochondria;

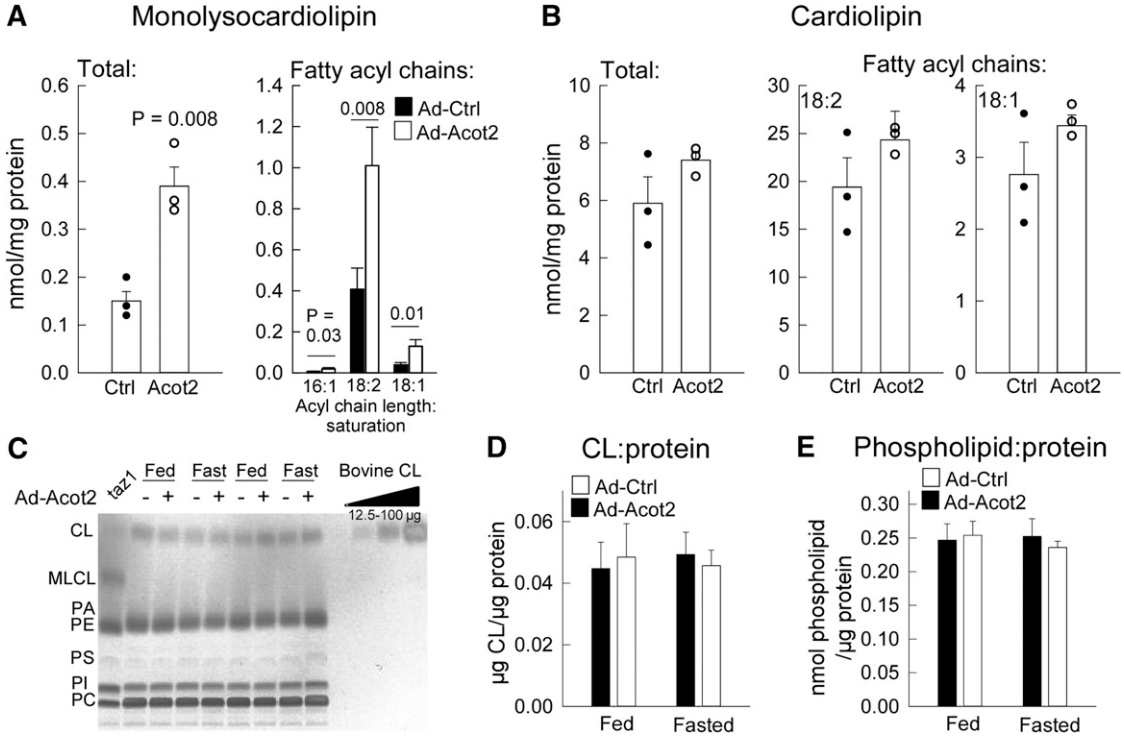

Fig. 4. Acot2 overexpression increases MLCL but not total CL in liver mitochondria. A, B: Shotgun lipidomics analysis of total MLCL and total CL in liver mitochondria from fed mice. Circles represent individual values, bars are the mean + SEM. Also shown is the total abundance of the major fatty acyl chains. *P* values: unpaired *t*-test, n = 3/group. The full dataset can be found in the supplementary data. C: Representative thin layer chromatographic analysis of total levels of MLCL, CL, phosphatidylethanolamine (PE), phosphatidylserine (PS), phosphatidylinositol (PI), and phosphatidylcholine (PC) in liver mitochondria. Similar results were obtained in six additional samples/groups. A sample from tafazzin deleted yeast is included as a positive control for MLCL. D: Total CL content/liver mitochondrial protein (n = 8/group). E: Total phospholipid content/liver mitochondrial protein (n = 8/group).

maximal ADP-stimulated JO_2 was elevated with 5 μM and to a lesser extent with 20 μM PCoA (+ malate + carnitine) (Fig. 5C). There was only a small difference in ADP-stimulated JO_2 with 5 and 20 μM PCoA. The dynamic range of the JO_2 response could be expanded by using MCoA (+ carnitine + malate). For all concentrations of MCoA, there was a tendency for higher phosphorylating (saturating ADP) JO_2 in Ad-Acot2 mitochondria. However, the difference between Ad-Ctrl and Ad-Acot2 was most pronounced, and was significant, at the lowest (5 μM) [MCoA] (Fig. 5D). Altogether, the experiments under phosphorylating conditions, using nonlipid or lipid substrates, suggest that overexpressed Acot2 specifically impacts FAO, and predominantly does so at low FA load.

To test for the presence of a FA export-activation-uptake cycle, palmitoyl-L-carnitine (PCarn) was used as the substrate, bypassing the CPT system. CoA was omitted from the reaction; thus, a cycle of FA export-activation-uptake would not be supported. This differs from the above PCoA and MCoA reactions which included carnitine to allow uptake of the activated FA into mitochondria, and also contained a source of CoA outside of mitochondria (cleaved from PCoA or MCoA); thus, the PCoA and MCoA reactions were capable of supporting a FA efflux-activation-uptake pathway. When PCarn was used, there were no significant differences between Ad-Ctrl and Ad-Acot2 mitochondria in phosphorylating JO_2 with 5 or 20 μM PCarn (Fig. 5E); however, there was a tendency for lower phosphorylating JO_2 with 20 μM PCarn. We further tested for a FA export-activation-uptake cycle by adding CoA to the PCarn reaction, as done previously in skeletal muscle mitochondria (17). However, the resulting JO_2 rates were highly variable even between replicates, and even when different [CoA] were tested (not shown). Nonetheless, the higher phosphorylating JO_2 in Ad-Acot2 mitochondria supplied with PCoA or MCoA, but not with PCarn, suggests that activation of FA on the outer mitochondrial membrane is required for the higher JO_2 when Acot2 is overexpressed.

To assess mitochondrial bioenergetics under conditions of intact flux control, JO_2 experiments were conducted in intact hepatocytes isolated from fed Ad-Ctrl and Ad-Acot2 mice 7 days after adenovirus injection. Basal JO_2 and extracellular acidification rate (ECAR) (the Seahorse instrument measures $[H^+]$ in the extracellular milieu, providing an estimate of glycolytic flux) of hepatocytes in DMEM + 5 mM glucose were each similar between Ad-Ctrl and Ad-Acot2 cells (**Fig. 6A**). With addition of 100 or 200 μM palmitate, JO_2 increased to the same extent and with similar kinetics in Ad-Ctrl and Ad-Acot2 cells (Fig. 6B). The increase in JO_2 was prevented by 75 μM etomoxir, which inhibits CPT1 (not shown). The accompanying changes in

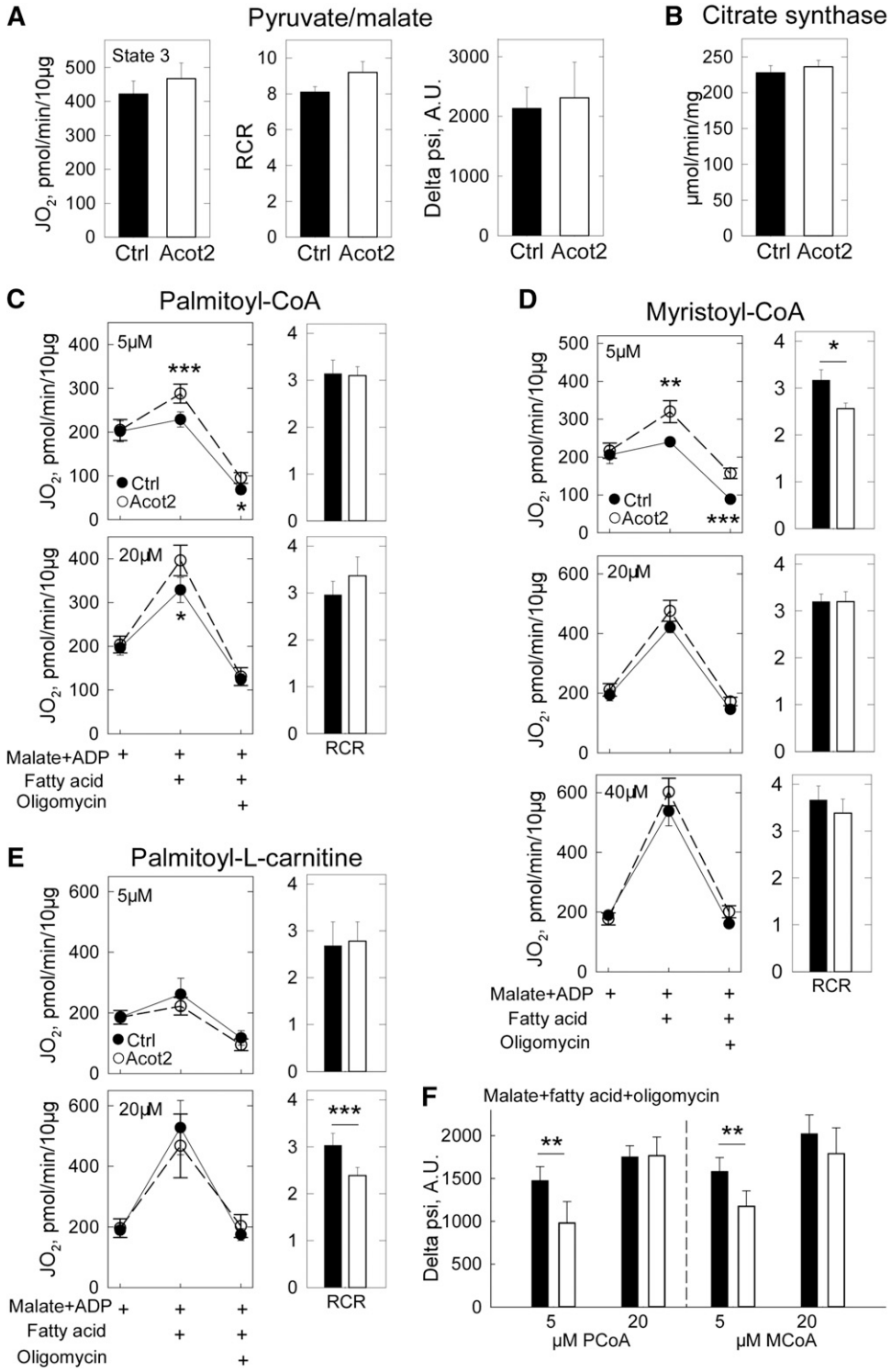

Fig. 5. Acot2 facilitates FAO and increases proton leak in liver mitochondria. A: State 3 oxygen consumption rate (JO_2) which is the maximal ADP-stimulated JO_2, RCR (state 3/state 4 which is the maximal JO_2 in the presence of oligomycin), and proton-motive force (delta psi) in liver mitochondria from fed mice supplied with saturating pyruvate/malate (10 mM/5 mM) and ADP. Oligomycin was used to obtain the state 4 rate (not shown). A.U., arbitrary units. n = 5/group. B: Citrate synthase in liver mitochondria from fed mice. C–E: JO_2 measured following addition of saturating ADP, then FA substrate, then oligomycin (in that order). Malate was already present when mitochondrial suspensions were added to the Seahorse plate. RCR: ratio of JO_2 in the presence of malate + ADP + FA to JO_2 in the presence of malate + ADP + FA + oligomycin. $^*P = 0.05$, $^{**}P = 0.01$, $^{***}P < 0.002$; unpaired *t*-test; n = 6–8/group. F: Proton-motive force. $^{**}P < 0.02$, unpaired *t*-test, n = 5/group. A–F: Black symbols/bars, Ad-Ctrl; open bars/symbols, Ad-Acot2.

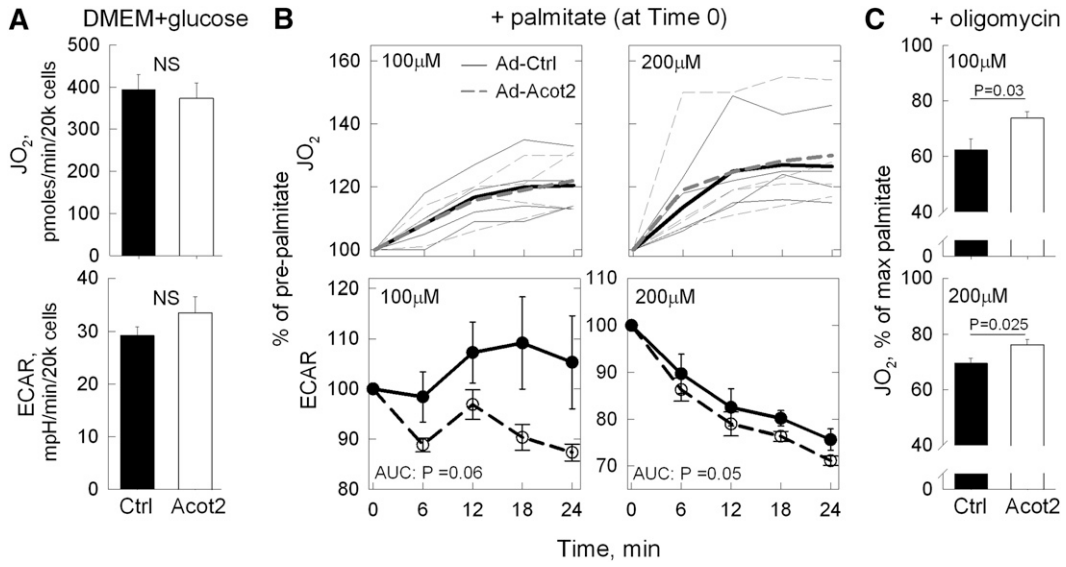

Fig. 6. Acot2 facilitates FAO and increases proton leak in hepatocytes. A–C: Data from each mouse is the average of five or six replicates (n = 4 mice/group); measurements were taken from 2 min recordings made every 6 min; all JO_2 rates are minus the JO_2 following antimycin injection (i.e., the nonmitochondrial JO_2). A: Measurement of JO_2 and ECAR in primary hepatocytes incubated in DMEM + 5 mM glucose. Values are the mean ± SEM. B: JO_2 and ECAR, expressed as percentage of values in DMEM + glucose, in primary hepatocytes after addition of palmitate (at time 0). In JO_2 panels, thin lines show the average response in each preparation, and the thick lines show the average of all preparations. Ad-Ctrl and Ad-Acot2 were not significantly different. In ECAR panels (symbols: mean ± SEM), the response was analyzed as the area under the curve (AUC). *P* values: unpaired *t*-test. C: JO_2 (mean ± SEM) after addition of oligomycin to block the ATP synthase. JO_2 is expressed as a percentage of the preoligomycin rate (i.e., the time = 24 min palmitate rate). *P* values, unpaired *t*-test.

the ECAR were also considered, because a switch to FA as the oxidizable substrate would be expected to lower glycolytic flux. In Ad-Acot2 hepatocytes, ECAR decreased by ~10% with 100 μM palmitate and by ~30% with 200 μM palmitate. In Ad-Ctrl cells, ECAR was unchanged 24 min after adding 100 μM palmitate, and was decreased by ~24% with 200 μM palmitate, which is significantly less than in Ad-Acot2 hepatocytes (Fig. 6B). These findings suggest a more efficient utilization of FA for ATP production by Acot2 mitochondria.

Oligomycin, which inhibits the ATP synthase thereby maximizing leak-dependent JO_2, was used to test whether Acot2 overexpression introduced a proton leak pathway. Proton leak-dependent JO_2 (i.e., oligomycin-insensitive JO_2) was significantly higher in Ad-Acot2 mitochondria supplied with 5 or 20 μM PCoA; this increase was in proportion to the higher ADP-stimulated JO_2 such that the ratio of ADP-stimulated to oligomycin-insensitive JO_2 RCR was similar in Ad-Ctrl and Ad-Acot2 mitochondria (Fig. 6C). However, proton-motive force measured in the presence of oligomycin was lower in Ad-Acot2 liver mitochondria for 5 μM PCoA only (Fig. 5F), suggesting that greater proton leak could occur in Ad-Acot2 liver mitochondria. Similar results were obtained with 5 μM MCoA, although in this case the RCR was lower in Ad-Acot2 mitochondria (Fig. 5D). In mitochondria supplied with PCarn, there was a tendency for a higher oligomycin-insensitive JO_2 with 20 μM PCarn in Ad-Acot2 mitochondria, and the RCR was significantly lower (Fig. 5E). In hepatocytes, leak-dependent JO_2, expressed as a fraction of JO_2 just prior to oligomycin addition, was higher in Ad-Acot2 cells for both 100 and 200 μM palmitate (Fig. 6C). The oligomycin-insensitive JO_2 was also higher in Ad-Acot2 cells when considered as the absolute JO_2. These findings in mitochondria and cells indicate that Acot2 overexpression introduced a leak-dependent pathway.

DISCUSSION

Mitochondrial Acots, by virtue of their substrate specificity, are poised to modulate mitochondrial FAO. Here we investigated, for the first time, the biological role of Acot2 in a tissue that robustly oxidizes FA. The biological role of Acot2 is of interest in the context of a broader understanding of how mitochondrial FAO is regulated and in the context of the reported association between mitochondrial FAO and cellular metabolic functions such as insulin signaling and lipid storage. Using hepatic Acot2 overexpression we demonstrate at the whole-animal level and in isolated mitochondria that Acot2 facilitates mitochondrial FAO, possibly through an efflux-activation-uptake circuit that would be driven by the release of FA by Acot2. Our experiments do not support a broader effect of Acot2 on mitochondrial function, in contrast to Acot15 (9). Experiments in mitochondria and hepatocytes also show that Acot2 can contribute to proton leak in mitochondria, and Tg depletion from the liver of mice overexpressing Acot2 may be due to increased energy expenditure due to uncoupled respiration.

Overexpressed Acot2 facilitates mitochondrial FAO

The observations in fed animals and tissue samples from fed mice indicate that overexpressed Acot2 leads to enhanced mitochondrial FAO. The lower RQ during the light phase in fed Ad-Acot2 mice clearly demonstrates a shift in substrate utilization toward increased use of FA substrate, but only during the daytime when there is normally greater utilization of FA substrate in rodents. The elevated β-hydroxybutyrate measured during the day in fed Ad-Acot2 mice suggests that the lower RQ was due, at least in part, to greater hepatic FAO. The liver acyl-carnitine profile suggests that mitochondrial uptake of FA was increased; the higher levels of long-chain acyl-carnitines may reflect reversal of CPT2, with reformation of carnitine esters from medium- or long-chain (but not short-chain) acyl-CoAs (35, 36). It should be noted that skeletal muscle Acot2 protein expression was not elevated in Ad-Acot2 mice, suggesting that FA uptake and utilization in skeletal muscle was similar to that for Ad-Ctrl mice; thus skeletal muscle seems unlikely to be a driver of the higher FA utilization in these mice.

The mitochondrial morphology findings provide further support, albeit indirect, for elevated FAO in Ad-Acot2 liver. In Ad-Ctrl mice, fasting caused liver mitochondria to elongate, as previously reported (37). This response was absent in Ad-Acot2 liver; thus mitochondria from fasted Ad-Acot2 mice were relatively fragmented. Saturated FA has been shown in C2C12 cells to fragment mitochondria (38). We speculate that a greater abundance of FA within and in close proximity to the mitochondria in Ad-Acot2 liver stimulated fission which countered the elongation of mitochondria that would have occurred with fasting.

Findings in isolated mitochondria support an ability of Acot2 to specifically enhance FAO. This is evidenced by the higher phosphorylating JO_2 with PCoA or MCoA substrates and lack of any differences from Ad-Ctrl when nonlipid substrates were supplied. That the increased phosphorylating JO_2 was most robust in Ad-Acot2 mitochondria at lower substrate concentrations agrees with the low K_m of Acot2. The lesser effects of Ad-Acot2 with higher FA concentrations may reflect either: *1*) substrate inhibition of Acot2 at high substrate concentrations; *2*) pathway saturation; or *3*) utilization of the FA products by other pathways. The latter possibility is supported by the expansion of the MLCL pool in Ad-Acot2 mitochondria.

Experiments in intact hepatocytes isolated from Ad-Ctrl and Ad-Acot2 mice demonstrated that Acot2 had no effect on basal JO_2, or on ECAR, when hepatocytes were supplied with nonlipid substrate (DMEM and glucose). This further supports that Acot2 overexpression did not broadly impact mitochondrial substrate oxidation, which contrasts with the role of Acot15 (9). This result also suggests that Acot2 overexpression did not lead to an additional energetic demand imposed on the cells. When hepatocytes were supplied with palmitate, the magnitude of the rise in JO_2 was similar in Ad-Ctrl and Ad-ACot2 cells. However the ECAR changes upon palmitate addition differed between Ad-Ctrl and Ad-Acot2 cells. If ATP demand is assumed to have remained constant, the lack of a drop in ECAR in Ad-Ctrl cells and the presence of a drop in ECAR in Ad-Acot2 cells could be interpreted as a lesser ability of Ad-Ctrl cells to synthesize ATP from the lipid substrate. It is noteworthy that the lower palmitate concentration (100 μM) better distinguished the Ad-Acot2 cells from the Ad-Ctrl cells, although this was evident in the ECAR response only. In an attempt to reveal a difference in JO_2 between Ad-Ctrl and Ad-Acot2 cells, lower concentrations of palmitate were used but were without a clear effect on JO_2 in either cell type, and thus were not helpful experimentally. Overnight incubation of cells in 300 μM palmitate:oleate, which increased Tg levels, also did not lead to differences in the JO_2 response to palmitate between Ad-Ctrl and Ad-Acot2 cells (not shown). In the context of the findings in vivo and in mitochondria, we conclude that the lack of a difference between Ad-Ctrl and Ad-Acot2 cells in the JO_2 response to palmitate suggests that Acot2 is highly regulated and that its regulation is linked to cellular conditions that were not replicated in isolated hepatocytes. In isolated mitochondria, this regulation could be overcome by the absence of various pathway control mechanisms.

Mechanistic insights into the Acot2-mediated enhancement of FAO

We were able to rule out changes in mitochondrial content and changes in key mitochondrial proteins as explanations for the lower in vivo RQ in fed Ad-Acot2 mice. The possibility that overexpressed Acot2 could modify CL metabolism was particularly important to consider in light of the association of Acot15 with CL metabolism (9). The expanded MLCL pool in Ad-Acot2 mitochondria certainly indicates that Acot2 can provide substrate for nonFAO reactions. Yet, because total CL was largely unchanged, the changes in FAO in Ad-Acot2 mice are unlikely to be related to changes in CL.

On the other hand, the analysis of CL and MLCL provides further support for a role for Acots in CL metabolism. MLCL is an intermediate formed during the normal acyl chain remodeling process that occurs for CL after synthesis, and may also be generated during CL degradation. Targeted analyses are needed to distinguish between a direct role for Acot2 in CL metabolism (remodeling or degradation) versus an indirect role (e.g., to provide FAs that are then incorporated into CL by acyl chain remodeling). The latter possibility is indeed supported by higher levels of some phosphatidylethanolamine and phosphatidylcholine species in Ad-Acot2 mitochondria (not shown). It is also possible that the elevated levels of MLCL are due to destabilization of the CL remodeling enzyme tafazzin; yet, any destabilization would be modest because total CL was not robustly different (and even tended to be higher) in Ad-Acot2 mitochondria. Moreover, Ad-Acot2 mitochondria did not show any of the morphological abnormalities observed in mitochondria from tafazzin knockout mice (39). A final possibility is that a greater abundance of FA in Ad-Acot2 mitochondria drove CL remodeling/degradation. Thus, it is clear that more in-depth studies are needed to elucidate the precise role of Acot2, and indeed also of Acot15, in CL metabolism.

Using isolated mitochondria, we aimed to test whether the FA released from Acot2 was effluxed from mitochondria, then reactivated on the outer mitochondrial membrane and taken back up by mitochondria to be potentially oxidized (33). The cost of this mechanism would be the ATP required for reactivation. On the other hand, this mechanism would allow Acot2 to facilitate FAO by relieving any inhibitory effects caused by a build-up of long-chain fatty acyl-CoA esters in the matrix (4–6). That higher phosphorylating JO_2 was observed in Ad-Acot2 mitochondria supplied with PCoA or MCoA, but not with PCarn, supports such a mechanism. Moreover, the tendency in Ad-Acot2 mitochondria supplied with 20 μM PCarn to have lower phosphorylating JO_2 and higher oligomycin-insensitive JO_2 (leading to significantly lower RCR) demonstrates the ability for Acot2 to siphon substrate away from oxidation pathways. In fact, the PCarn experiments provide the only FA conditions where phosphorylating JO_2 tended to be lower in Ad-Acot2 mitochondria; again, this would reflect the removal, by Acot2, of substrate from β-oxidation. Thus, the PCarn experiments indirectly support the need for an efflux-activation-uptake circuit to drive the higher phosphorylating JO_2 that was observed with PCoA and MCoA and saturating ADP.

The FA products of the Acot2 reaction could potentially cycle in the inner membrane, providing a return path for protons and leading to greater leak-dependent respiration (34). The experiments in mitochondria and cells using oligomycin clearly demonstrate that Acot2 is capable of contributing an additional pathway for proton return. VO_2 in fed mice was not measurably altered by Acot2 overexpression, even toward the end of the light phase of the day when the FA products of the Acot2 reaction could have accumulated to thereby cause greater leak-dependent respiration. However, a small difference in energy expenditure in fed Ad-Acot2 mice (due to greater uncoupled respiration) in Ad-Acot2 liver, may have been below the level of detection of indirect calorimetry. However, the failure of Tg to markedly accumulate in fasted Ad-Acot2 liver, as it did in Ad-Ctrl liver, may be the result of elevated energy expenditure in the liver due to an acceleration of uncoupled respiration by liver mitochondria. Whether this would be caused by increased activity of Acot2 or by the gradual accumulation of FAs in the matrix cannot be known from the present study. We can, however, conclude that increased proton return is not an obligatory outcome of Acot2 overexpression because, in hepatocytes, the JO_2 response to palmitate was not higher in Ad-Acot2 cells, even though the subsequent oligomycin-insensitive JO_2 was higher.

In conclusion, our experiments using Acot2 overexpression indicate that Acot2 can enhance the hepatic oxidation of FA in mitochondria, and also has the potential to contribute to proton leak. Differently from Acot15, the effect of Acot2 is specific to FAO. The low K_m of Acot2 and the functional data both support a niche for Acot2 in conditions when ATP demand is low and FA is the prevailing substrate for oxidation. Finally, we speculate that the ability of Acot2 to mitigate hepatic steatosis in fasted mice suggests that any individuals having hypomorphic Acot2 alleles would be at an increased risk for ectopic lipid accumulation.

The authors thank Dr. Jan Hoek (Thomas Jefferson University, Pathology) for the use of equipment to isolate hepatocytes and Tim Schneider (Thomas Jefferson University, Pathology) for electron microscopy sample sectioning and imaging.

REFERENCES

1. Koves, T. R., J. R. Ussher, R. C. Noland, D. Slentz, M. Mosedale, O. Ilkayeva, J. Bain, R. Stevens, J. R. Dyck, C. B. Newgard, et al. 2008. Mitochondrial overload and incomplete fatty acid oxidation contribute to skeletal muscle insulin resistance. *Cell Metab.* **7:** 45–56.
2. Muoio, D. M., and P. D. Neufer. 2012. Lipid-induced mitochondrial stress and insulin action in muscle. *Cell Metab.* **15:** 595–605.
3. Muoio, D. M., R. C. Noland, J. P. Kovalik, S. E. Seiler, M. N. Davies, K. L. DeBalsi, O. R. Ilkayeva, R. D. Stevens, I. Kheterpal, J. Zhang, et al. 2012. Muscle-specific deletion of carnitine acetyltransferase compromises glucose tolerance and metabolic flexibility. *Cell Metab.* **15:** 764–777.
4. van Eunen, K., S. M. Simons, A. Gerding, A. Bleeker, G. den Besten, C. M. Touw, S. M. Houten, B. K. Groen, K. Krab, D. J. Reijngoud, et al. 2013. Biochemical competition makes fatty-acid beta-oxidation vulnerable to substrate overload. *PLOS Comput. Biol.* **9:** e1003186.
5. Shug, A., E. Lerner, C. Elson, and E. Shrago. 1971. The inhibition of adenine nucleotide translocase activity by oleoyl CoA and its reversal in rat liver mitochondria. *Biochem. Biophys. Res. Commun.* **43:** 557–563.
6. Woldegiorgis, G., S. Y. Yousufzai, and E. Shrago. 1982. Studies on the interaction of palmitoyl coenzyme A with the adenine nucleotide translocase. *J. Biol. Chem.* **257:** 14783–14787.
7. Hunt, M. C., K. Solaas, B. F. Kase, and S. E. Alexson. 2002. Characterization of an acyl-coA thioesterase that functions as a major regulator of peroxisomal lipid metabolism. *J. Biol. Chem.* **277:** 1128–1138.
8. Tillander, V., E. Arvidsson Nordström, J. Reilly, M. Strozyk, P. P. Van Veldhoven, M. C. Hunt, and S. E. Alexson. 2014. Acyl-CoA thioesterase 9 (ACOT9) in mouse may provide a novel link between fatty acid and amino acid metabolism in mitochondria. *Cell. Mol. Life Sci.* **71:** 933–948.
9. Zhuravleva, E., H. Gut, D. Hynx, D. Marcellin, C. K. Bleck, C. Genoud, P. Cron, J. J. Keusch, B. Dummler, M. D. Esposti, et al. 2012. Acyl coenzyme A thioesterase Them5/Acot15 is involved in cardiolipin remodeling and fatty liver development. *Mol. Cell. Biol.* **32:** 2685–2697.
10. Zhang, Y., Y. Li, M. W. Niepel, Y. Kawano, S. Han, S. Liu, A. Marsili, P. R. Larsen, C. H. Lee, and D. E. Cohen. 2012. Targeted deletion of thioesterase superfamily member 1 promotes energy expenditure and protects against obesity and insulin resistance. *Proc. Natl. Acad. Sci. USA.* **109:** 5417–5422.
11. Wei, J., H. W. Kang, and D. E. Cohen. 2009. Thioesterase superfamily member 2 (Them2)/acyl-CoA thioesterase 13 (Acot13): a homotetrameric hotdog fold thioesterase with selectivity for long-chain fatty acyl-CoAs. *Biochem. J.* **421:** 311–322.
12. Claypool, S. M., and C. M. Koehler. 2012. The complexity of cardiolipin in health and disease. *Trends Biochem. Sci.* **37:** 32–41.
13. King, K. L., M. E. Young, J. Kerner, H. Huang, K. M. O'Shea, S. E. Alexson, C. L. Hoppel, and W. C. Stanley. 2007. Diabetes or peroxisome proliferator-activated receptor alpha agonist increases mitochondrial thioesterase I activity in heart. *J. Lipid Res.* **48:** 1511–1517.
14. Stavinoha, M. A., J. W. RaySpellicy, M. F. Essop, C. Graveleau, E. D. Abel, M. L. Hart-Sailors, H. J. Mersmann, M. S. Bray, and M. E. Young. 2004. Evidence for mitochondrial thioesterase 1 as a peroxisome proliferator-activated receptor-alpha-regulated gene in cardiac and skeletal muscle. *Am. J. Physiol. Endocrinol. Metab.* **287:** E888–E895.
15. Hunt, M. C., S. E. Nousiainen, M. K. Huttunen, K. E. Orii, L. T. Svensson, and S. E. Alexson. 1999. Peroxisome proliferator-induced long chain acyl-CoA thioesterases comprise a highly conserved novel multi-gene family involved in lipid metabolism. *J. Biol. Chem.* **274:** 34317–34326.

16. Hunt, M. C., Y. Z. Yang, G. Eggertsen, C. M. Carneheim, M. Gafvels, C. Einarsson, and S. E. Alexson. 2000. The peroxisome proliferator-activated receptor alpha (PPARalpha) regulates bile acid biosynthesis. *J. Biol. Chem.* **275:** 28947–28953.
17. Seifert, E. L., V. Bezaire, C. Estey, and M. E. Harper. 2008. Essential role for uncoupling protein-3 in mitochondrial adaptation to fasting but not in fatty acid oxidation or fatty acid anion export. *J. Biol. Chem.* **283:** 25124–25131.
18. Svensson, L. T., S. E. Alexson, and J. K. Hiltunen. 1995. Very long chain and long chain acyl-CoA thioesterases in rat liver mitochondria. Identification, purification, characterization, and induction by peroxisome proliferators. *J. Biol. Chem.* **270:** 12177–12183.
19. Duarte, A., A. F. Castillo, R. Castilla, P. Maloberti, C. Paz, E. J. Podesta, and F. Cornejo Maciel. 2007. An arachidonic acid generation/export system involved in the regulation of cholesterol transport in mitochondria of steroidogenic cells. *FEBS Lett.* **581:** 4023–4028.
20. Maloberti, P., R. Castilla, F. Castillo, F. Cornejo Maciel, C. F. Mendez, C. Paz, and E. J. Podesta. 2005. Silencing the expression of mitochondrial acyl-CoA thioesterase I and acyl-CoA synthetase 4 inhibits hormone-induced steroidogenesis. *FEBS J.* **272:** 1804–1814.
21. Seifert, E. L., C. Estey, J. Y. Xuan, and M. E. Harper. 2010. Electron transport chain-dependent and -independent mechanisms of mitochondrial H2O2 emission during long-chain fatty acid oxidation. *J. Biol. Chem.* **285:** 5748–5758.
22. Rogers, G. W., M. D. Brand, S. Petrosyan, D. Ashok, A. A. Elorza, D. A. Ferrick, and A. N. Murphy. 2011. High throughput microplate respiratory measurements using minimal quantities of isolated mitochondria. *PLoS ONE.* **6:** e21746.
23. Christie, W. W., and X. Han. 2010. Lipid Analysis: Isolation, Separation, Identification and Lipidomic Analysis. Oily Press, Bridgwater, UK.
24. Han, X., K. Yang, and R. W. Gross. 2008. Microfluidics-based electrospray ionization enhances the intrasource separation of lipid classes and extends identification of individual molecular species through multi-dimensional mass spectrometry: development of an automated high-throughput platform for shotgun lipidomics. *Rapid Commun. Mass Spectrom.* **22:** 2115–2124.
25. Yang, K., H. Cheng, R. W. Gross, and X. Han. 2009. Automated lipid identification and quantification by multidimensional mass spectrometry-based shotgun lipidomics. *Anal. Chem.* **81:** 4356–4368.
26. Yang, K., and X. Han. 2011. Accurate quantification of lipid species by electrospray ionization mass spectrometry - Meet a key challenge in lipidomics. *Metabolites.* **1:** 21–40.
27. Claypool, S. M., Y. Oktay, P. Boontheung, J. A. Loo, and C. M. Koehler. 2008. Cardiolipin defines the interactome of the major ADP/ATP carrier protein of the mitochondrial inner membrane. *J. Cell Biol.* **182:** 937–950.
28. Claypool, S. M., J. M. McCaffery, and C. M. Koehler. 2006. Mitochondrial mislocalization and altered assembly of a cluster of Barth syndrome mutant tafazzins. *J. Cell Biol.* **174:** 379–390.
29. Rouser, G., S. Fkeischer, and A. Yamamoto. 1970. Two dimensional then layer chromatographic separation of polar lipids and determination of phospholipids by phosphorus analysis of spots. *Lipids.* **5:** 494–496.
30. Das, S., N. Hajnoczky, A. N. Antony, G. Csordas, L. D. Gaspers, D. L. Clemens, J. B. Hoek, and G. Hajnoczky. 2012. Mitochondrial morphology and dynamics in hepatocytes from normal and ethanol-fed rats. *Pflugers Arch.* **464:** 101–109.
31. Guan, H. P., J. L. Goldstein, M. S. Brown, and G. Liang. 2009. Accelerated fatty acid oxidation in muscle averts fasting-induced hepatic steatosis in SJL/J mice. *J. Biol. Chem.* **284:** 24644–24652.
32. Chicco, A. J., and G. C. Sparagna. 2007. Role of cardiolipin alterations in mitochondrial dysfunction and disease. *Am. J. Physiol. Cell Physiol.* **292:** C33–C44.
33. Himms-Hagen, J., and M. E. Harper. 2001. Physiological role of UCP3 may be export of fatty acids from mitochondria when fatty acid oxidation predominates: an hypothesis. *Exp. Biol. Med. (Maywood).* **226:** 78–84.
34. Schönfeld, P., L. Schild, and W. Kunz. 1989. Long-chain fatty acids act as protonophoric uncouplers of oxidative phosphorylation in rat liver mitochondria. *Biochim. Biophys. Acta.* **977:** 266–272.
35. Violante, S., L. Ijlst, H. van Lenthe, I. T. de Almeida, R. J. Wanders, and F. V. Ventura. 2010. Carnitine palmitoyltransferase 2: new insights on the substrate specificity and implications for acylcarnitine profiling. *Biochim. Biophys. Acta.* **1802:** 728–732.
36. Johnson, T. M., W. R. Mann, C. J. Dragland, R. C. Anderson, G. M. Nemecek, and P. A. Bell. 1995. Over-expression and characterization of active recombinant rat liver carnitine palmitoyltransferase II using baculovirus. *Biochem. J.* **309:** 689–693.
37. Gomes, L. C., G. Di Benedetto, and L. Scorrano. 2011. During autophagy mitochondria elongate, are spared from degradation and sustain cell viability. *Nat. Cell Biol.* **13:** 589–598.
38. Jheng, H. F., P. J. Tsai, S. M. Guo, L. H. Kuo, C. S. Chang, I. J. Su, C. R. Chang, and Y. S. Tsai. 2012. Mitochondrial fission contributes to mitochondrial dysfunction and insulin resistance in skeletal muscle. *Mol. Cell. Biol.* **32:** 309–319.
39. Acehan, D., F. Vaz, R. H. Houtkooper, J. James, V. Moore, C. Tokunaga, W. Kulik, J. Wansapura, M. J. Toth, A. Strauss, et al. 2011. Cardiac and skeletal muscle defects in a mouse model of human Barth syndrome. *J. Biol. Chem.* **286:** 899–908.